JOURNAL OF MATERIALS SCIENCE 19 (1984) 3786–3795

Production of metal–zirconium type amorphous wires and their mechanical strength and structural relaxation

A. INOUE, T. MASUMOTO
The Research Institute for Iron, Steel and Other Metals, Tohoku University, Sendai 980, Japan

N. YANO
Unitika Research and Development Center, Unitika Ltd, Uji 611, Japan

Metal–metal type amorphous wires with a good ductility were produced in the M–Zr (M = Cu, Cu–Nb and Cu–Ta) alloy systems by a technique using melt spinning into rotating water. The formation of the amorphous wires is limited to a narrow range of 35 to 40 at % zirconium where the critical sample thickness for the formation of an amorphous phase is above about 100 μm and the amount of copper replaced by niobium or tantalum is less than about 7 and 5 at %, respectively. The wires have a circular cross-section and a rather smooth peripheral surface. Their diameters are in the range of 0.07 to 0.15 mm. The Vickers hardness, H_v, and tensile strength, σ_f, are of the order of 425 to 440 DPN and 1670 to 1810 MPa. The elongation to fracture, ϵ_f, is about 2.4 to 2.7%. Cold drawing to about 30% reduction in area results in increases in σ_f and ϵ_f by about 10% and 35%, respectively. Furthermore, the addition of 5 at % niobium results in decreases in σ_f and H_v by about 14% and 4%, respectively, without detriment to the good bending ductility. Owing to the faster quench rates of the wire samples, caused by the inherent differences in the solidification process of the ejected melt as well as in the manner of cooling after solidification, the amorphous wires have been found to exhibit a considerably higher relaxation enthalpy value, ΔH, and a lower temperature for the onset of structural relaxation as compared with the amorphous ribbon having the same thickness as the diameter of the wire, demonstrating that the amorphous wires possess a higher degree of structural disorder.

1. Introduction

Continuous amorphous wires with diameters ranging from about 70 to 250 μm have recently been reported to be fabricated in technologically important iron- [1, 2], cobalt- [3] and nickel- [4] based alloys as well as in noble metal- (palladium- [5] and platinum- [6]) based alloys by a newly developed technique using melt spinning into rotating water [5, 7, 8]. The maximum length of the iron-based amorphous wire fabricated in one ejecting operation is at present as long as several kilometres. The finding explodes the previous conception for the melt-quenched amorphous materials, in which the maximum sample thickness is limited to less than about 50 μm, and leads to a marked enhancement of the engineering value of the amorphous metallic materials. The amorphous wires in various alloy systems produced to date have been reported to exhibit high mechanical strengths, good ductility and high corrosion resistance, which are the same level as those for the ribbon materials with a thickness less than about 50 μm [1–6]. Additionally, the iron- and cobalt-based amorphous wires have been found to

0022–2461/84 $03.00 + .12

possess unique magnetic characteristics, which are different from those for the ribbon materials, owing to a different magnetic domain structure caused by the different solidification process [9]. Owing to the many advantages, the practical use of the amorphous wires as soft ferromagnetic, high-strength and/or high corrosion resistance materials appears to be highly promising [10].

However, all the amorphous wires produced to date [1–6] are limited to the metal–metalloid system containing metalloid elements of boron, phosphorus, carbon and silicon and there is no information available on the formation and characteristics of metal–metal type amorphous wires, in spite of the expectation that they might exhibit useful electrical properties such as superconductivity. We examined systematically the maximum sample thickness for the formation of an amorphous single phase in Cu–Zr, Ni–Zr and Co–Zr binary alloys which are expected to possess a high amorphous-forming ability in metal–metal alloy systems and found that an amorphous wire is formed in Cu–Zr alloys which exhibit a critical sample thickness larger than about 100 μm. The purpose of this paper is to present the composition dependence of the critical sample thickness for the formation of an amorphous single phase in Cu–Zr, Ni–Zr and Co–Zr alloys, the composition range and the spinning condition in which an amorphous wire is formed, and the peripheral structure, mechanical strengths and thermal stability of the wires.

2. Experimental methods

2.1. Alloys

The specimens used in the present work were $Cu_{100-x}Zr_x$ (x = 25 to 70 at%), $Ni_{100-x}Zr_x$ (x = 25 to 60 at%) and $Co_{100-x}Zr_x$ (x = 30 to 60 at%) binary and $(Cu–Zr)_{100-x}Nb_x$ ($x \leqslant 15$ at%) and $(Cu–Zr)_{100-x}Ta_x$ ($x \leqslant 15$ at%) ternary alloys. Their alloy ingots were prepared under a purified and gettered argon atmosphere in an arc furnace on a water-cooled copper mould from zirconium (99.6 wt%), electrolytic pure metals of copper (99.9 wt%), nickel (99.97 wt%) and cobalt (99.5 wt%) and pure refractory metals of niobium (99.5 at%) and tantalum (99.5 wt%). The weight of the mixture melted in one run was about 30 g. The ingots were repeatedly turned over and remelted to ensure homogeneity. The compositions of alloys reported are the nominal ones since the losses during melting were negligible.

2.2. The critical sample thickness for the formation of an amorphous phase

From the master ingots prepared by the above-described method, long ribbons with a continuous variation in thickness in the range 20 to 200 μm were produced using the modified melt-quenching apparatus which enables the copper roller (20 cm diameter) revolving at high speeds (3000 to 5000 rpm) to stop in a short time (1 to 2 sec). The short time required for the roller to stop was chosen so as to eject the molten alloy through a small orifice by argon pressure. Such a rapid stop was achieved by a simultaneous operation of dynamic brake and disc brake attached to the shaft of the copper roller. A detailed description of the apparatus used is given by Hagiwara *et al.* [11]. With decreasing rotation speed of the roller, the thickness of the as-quenched samples increases continuously in the range 20 to 200 μm, but the width is almost constant ($\simeq$ 1.5 mm). The critical thickness was taken as that thickness where a crystalline particle on the ribbon surface could be just observed by the optical microscope at the magnification of $\times$ 100. The critical thickness identified by optical microscopy was confirmed to agree well with those from X-ray and differential scanning calorimetry (DSC) analyses. The subsequent detailed procedures for determining the critical thickness are the same as those described by Hagiwara *et al.* [11, 12].

2.3. Amorphous wires

Amorphous wires of about 0.07 to 0.15 mm diameter were prepared from the master ingots by a melt-spinning apparatus in which the melt is ejected through an orifice into rotating water in a drum. The details of the apparatus have been described previously [5, 8]. Typically, the amount of alloy melted in one run was about 1 g, the rotation speed of the drum (50 cm diameter) was about 300 rev min^{-1} and the depth of the cooling water was about 25 mm.

Structure of the as-quenched wires was examined using an X-ray diffractometer using Cu$K\alpha$ radiation in combination with an X-ray monochrometer. The wires were classified as amorphous when the X-ray intensity as a function of diffraction angle showed a typical liquid-like structure. The hardness and tensile strength of the wires were measured using a Vickers microhardness tester with a 100 g load and an Instron-type tensile-testing machine at a strain rate of 4.2×10^{-4} sec^{-1},

respectively. The glass transition temperature (T_g), the heat of structural relaxation (ΔH) and crystallization temperature (T_x) were examined with a differential scanning calorimeter (DSC) at a heating rate of 40 K min^{-1}. The ductility was evaluated by measuring the radius of curvature at fracture in a simple bending test. The peripheral structure before and after cold drawing and the fracture surface were observed with a scanning electron microscope.

3. Results and discussion

3.1. The tendency to form the amorphous phase in Zr–M (M = Cu, Ni or Co)

In order to obtain information for a given alloy on its tendency to form the amorphous phase (this is essential for the production of an amorphous wire), we examined the critical sample thickness for the formation of amorphous Zr–M (M = Cu, Ni or Co) binary alloys. The critical sample thickness for the formation of amorphous Cu–Zr and Ni–Zr alloys as a function of zirconium concentration is plotted in Figs. 1 and 2. The critical thickness is the greatest (above 180 μm) for $Cu_{60-65}Zr_{35-40}$ and ($\simeq$ 90 μm) for $Ni_{65}Zr_{35}$, decreases with increasing or decreasing zirconium content and is

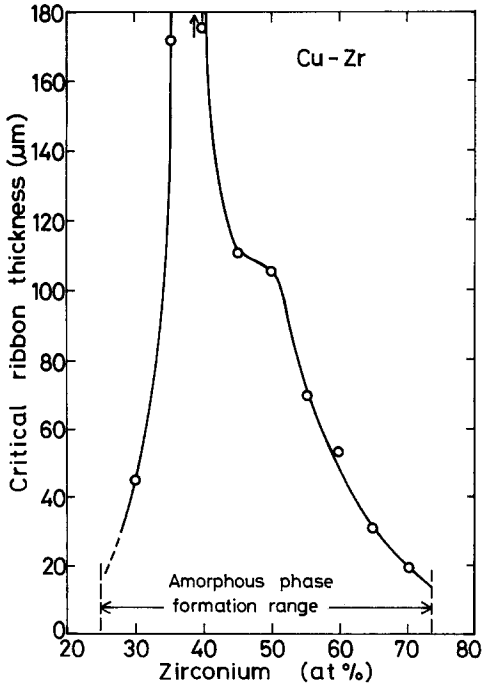

Figure 1 Composition range and the critical ribbon thickness for the formation of an amorphous single phase in Cu–Zr binary alloys.

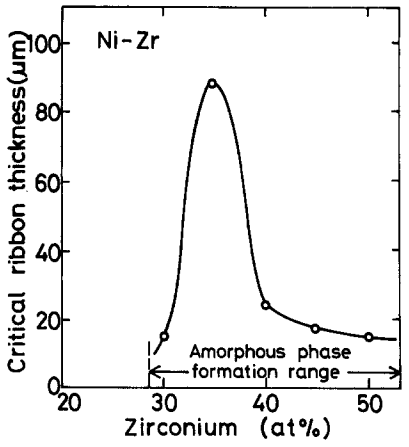

Figure 2 Composition range and the critical ribbon thickness for the formation of an amorphous single phase in Ni–Zr binary alloys.

about 15 to 20 μm near the boundary between the amorphous and crystalline phases, indicating that the tendency to form the amorphous phase has a marked compositional dependence. In addition, no amorphous single phase was found in the ribbons having thicknesses larger than about 50 μm over the whole composition range of Co–Zr system. Thus, the amorphous phase-forming ability is the greatest for Cu–Zr alloys, followed for Ni–Zr and then Co–Zr.

As described above, it was demonstrated that the amorphous phase-forming ability exhibits an extremely large compositional dependence even in the same alloy system, in addition to the marked difference among each alloy system (Cu–Zr, Ni–Zr and Co–Zr). Here we shall briefly investigate the reason for the significant change in the amorphous phase-forming ability with varying zirconium content for Cu–Zr alloys. An amorphous single phase is formed only in the case where liquid is supercooled below T_g without crystallization at T_m. Therefore, the amorphous phase-forming ability of metallic alloys is enhanced by increasing the reduced glass transition temperature (T_g/T_m), i.e. upon lowering the equilibrium freezing temperature and on increasing the rate at which the viscosity of the liquid increases with decreasing temperature [13–17]. Fig. 3 shows the measured values of T_g/T_m of Cu–Zr alloys as a function of zirconium content. The value of T_g/T_m shows a maximum value ($\simeq$ 0.64) at about 40 at% zirconium and decreases significantly with increasing or decreasing zirconium content. Such a marked composition dependence of T_g/T_m is very

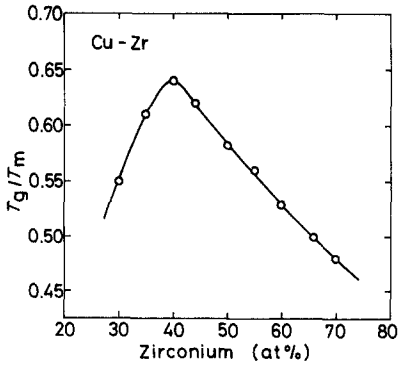

Figure 3 Composition dependence of the reduced glass transition temperature T_g/T_m of Cu–Zr alloys.

analogous to that of the critical sample thickness for the formation of an amorphous single phase shown in Fig. 1. Furthermore, Fig. 4 shows the relationship between T_g/T_m and the critical sample thickness for Cu–Zr binary alloys. There exists a strong correlation that the larger the T_g/T_m the larger is the critical sample thickness. From these data, it may be concluded that the large difference in the amorphous-forming ability can be interpreted in terms of T_g/T_m; the large amorphous-forming ability of $Cu_{60-65}Zr_{35-40}$ alloys is due to the low T_m and the rapid increase in the viscosity of the liquid with decreasing temperature (which are considered to be caused by the formation of short-range ordering due to the strong attractive interaction between copper and zirconium). It is well known [18, 19] that the short-range ordering by the attractive interaction among constituent elements results in an increase in T_g and the reductions in the free energy of the liquid and the melting point of the alloys.

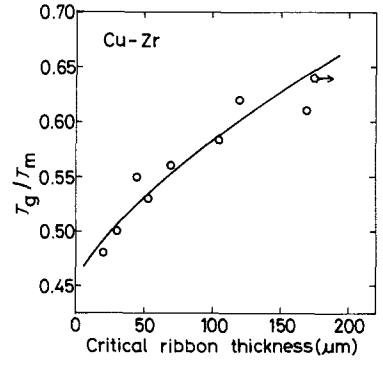

Figure 4 Correlation between the critical ribbon thickness for the formation of an amorphous single phase for Cu–Zr and Ni–Zr alloys and their reduced glass transition temperature T_g/T_m.

3.2. Production of Cu–Zr amorphous wires

The production of an amorphous wire was tried for the $Cu_{65}Zr_{35}$ and $Cu_{60}Zr_{40}$ alloys exhibiting an amorphous-forming critical thickness much larger than 100 μm. Fig. 5 shows typical scanning electron micrographs of the peripheral surface of $Cu_{65}Zr_{35}$ and $Cu_{60}Zr_{40}$ amorphous wires. It should be noted that metal–metal type amorphous wires with an almost completely circular cross-section can be produced in one operation by the present apparatus. The scatter in the diameters is less than about 12% for the wires of about 90 μm diameter and tends to increase with increasing wire diameter.

The main quenching parameters for the production of Cu–Zr amorphous wires with a good shape and uniformity were adjusted as follows:

1. the distance between the surface of water and the end of a quartz tube was less than about 3 mm and the ejecting angle against the surface of the water was about 80°,

2. the hole size of the quartz nozzle was 0.10 to 0.15 mm i.d.,

3. the temperature of the cooling water was approximately 278 K, and

4. the melt was ejected by an argon pressure of about 0.4 MPa from a temperature about 50 K above the liquidus temperature and the melt jet speed was estimated to be about 400 m min^{-1}.

Furthermore, it is very important to control precisely the ratio of the jet velocity to the water velocity in the drum because of the inherent instability of a cylindrical melt jet caused by a high surface tension and a low viscosity. Under the condition when the water velocity in the drum exceeds the jet velocity by about 15 to 20%, continuous Cu–Zr amorphous wires with a rather smooth surface are wound on the inner side of the drum.

In conclusion, the difference in the spinning conditions of the Cu–Zr wires and the metal–metalloid alloy wires such as Fe–Si–B, Fe–P–C and Co–Si–B systems may be summarized as follows:

1. the shorter distance between the end of a quartz tube and the surface of water;

2. the larger ejecting pressure;

3. the larger ejecting angle against the surface of water; and

4. the slightly lower rotation speed of the drum.

One can notice that these modifications of the spinning conditions result from the following differences in the liquid between Cu–Zr and the

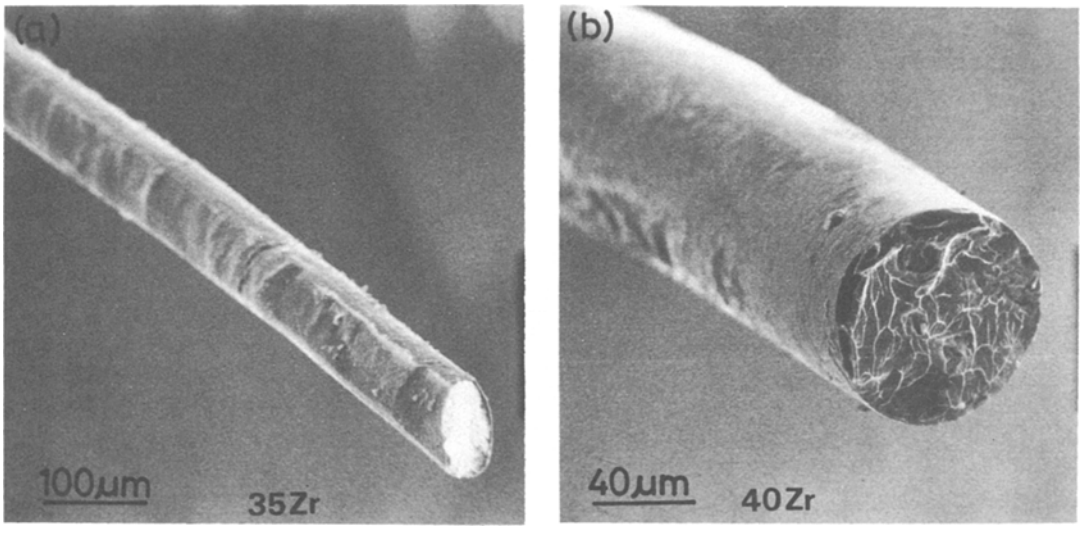

Figure 5 Scanning electron micrographs showing the peripheral surface of undrawn (a) $Cu_{65}Zr_{35}$ and (b) $Cu_{60}Zr_{40}$ amorphous wires.

metal–metalloid alloys; the molten jet of the Cu–Zr alloys is more reactive with oxygen in air and possesses a considerably lower viscosity as compared with those of the metal–metalloid alloys.

Within the present work, the formation of the amorphous wires in the Cu–Zr system is limited to a narrow range of 35 to 40 at% zirconium and no amorphous wire with no crystallinity is formed in Ni–Zr and Co–Zr alloys because of their considerably lower amorphous forming ability. In addition, the addition of niobium or tantalum was not detrimental to the formation of the Cu–Zr amorphous wires in the range less than about 7 at% for niobium and about 5 at% for tantalum. Further increase in niobium or tantalum content results in the formation of extremely brittle duplex-phase wires consisting of amorphous and crystalline phase owing to a marked decrease in the amorphous-forming ability.

3.3. Mechanical properties

Tensile fracture strength (σ_f), elongation to fracture including elastic elongation (ϵ_f), and Vickers hardness (H_v), of undrawn and drawn $Cu_{65}Zr_{35}$, $Cu_{60}Zr_{40}$, $(Cu_{0.65}Zr_{0.35})_{95}Nb_5$ and $(Cu_{0.60}Zr_{0.40})_{95}Nb_5$ amorphous wires are summarized in Table I, where T_g, T_x, the wire dia-

TABLE I Tensile fracture strength (σ_f), fracture elongation (ϵ_f) including elastic elongation, Vickers hardness (H_v), glass transition temperature (T_g), crystallization temperature (T_x), and wire diameter (D) for undrawn and drawn Cu–Zr amorphous wires. R is the reduction in cross-sectional area by drawing

Alloy composition	σ_f (MPa)	ϵ_f (%)	H_v (DPN)	T_g (K)	T_x (K)
$Cu_{65}Zr_{35}$					
$D = 135\,\mu m$	1670	2.4	425	758	770
$R = 28\%$	1850	3.3	–	–	–
$Cu_{60}Zr_{40}$					
$D = 110\,\mu m$	1810	2.7	440	740	754
$R = 26\%$	1950	3.6	–	–	–
$(Cu_{0.65}Zr_{0.35})_{95}Nb_5$					
$D = 105\,\mu m$	1865	2.2	440	–	–
$(Cu_{0.60}Zr_{0.40})_{95}Nb_5$					
$D = 95\,\mu m$	2100	2.4	460	–	–
Beryllium bronze 25 alloy	1274–1372	1–2	380–445	–	–

meter before drawing and the reduction in wire cross-section area by drawing, are also given. Here the strength values are the average of seven specimens and T_x is the temperature of onset of crystallization determined from the DSC curve. As seen in the table, σ_f, ϵ_f and H_v of the undrawn wires are 1670 MPa, 2.4% and 425 DPN, respectively, for $Cu_{65}Zr_{35}$, and 1810 MPa, 2.7% and 440 DPN for $Cu_{60}Zr_{40}$, indicating that the strength and elongation are slightly higher for $Cu_{60}Zr_{40}$ than for $Cu_{65}Zr_{35}$. Furthermore, one can see in the table that the addition of niobium results in an increase in σ_f and H_v and a decrease in ϵ_f, and the highest σ_f value attained for the metal–metal type undrawn amorphous wires is 2100 MPa for $(Cu_{0.6}Zr_{0.4})_{95}Nb_5$. Although the highest value is considerably lower than those for the metal–metalloid type amorphous wires of Fe–Si–B, Fe–P–C and Co–Si–B systems, the σ_f value is much higher than the highest value [20] of optimally age-hardened Cu–Be alloys.

There is no appreciable sample diameter effect on the value of σ_f in the diameter range 70 to 150 μm, but ϵ_f tends to increase by about 10% with increasing wire diameter. Such a sample size effect on strength and elongation is very similar to that for Fe–Si–B amorphous wires [1].

3.4. Effect of drawing on strength and elongation

The effect of cold drawing on the mechanical properties of the Cu–Zr amorphous wires was investigated to check for an improvement in wire strength and elongation. The $Cu_{65}Zr_{35}$ and $Cu_{60}Zr_{40}$ wires could be cold drawn from an initial diameter of 135 μm to a final diameter of 40 μm after multiple passes through several diamond dies without annealing treatments. Soapy water was used as a lubricant in the cold-drawing procedures. The Cu–Zr amorphous wires posses a good bending ductility, even after a cold-drawing as severe as about 91% reduction in cross-sectional area. As an example, the deformation structure of the cold-drawn $Cu_{65}Zr_{35}$ amorphous wire bent by pressing around the edge of a thin razor blade is shown in Fig. 6. Two families of deformation markings and rather large deformation steps appear near the bent edge. One makes an angle of about 45° to 50° to the longitudinal direction of the wire, while the other lies nearly perpendicular to it. It can also be seen that a large number of the deformation markings intersect each other and some are terminated by others. Furthermore, Fig. 6 shows that microcracks initiate at the point (marked with an arrow) where three slip markings intersected, suggesting that a high stress concentrated at the triple point.

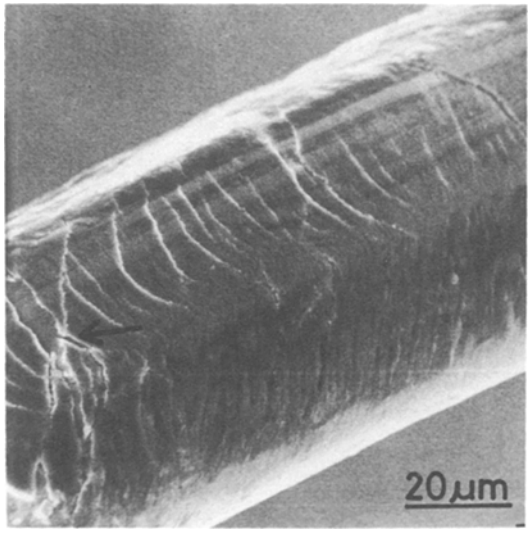

Figure 6 Scanning electron micrograph showing the deformation markings at the tip of $Cu_{65}Zr_{35}$ wire bent through 180°.

As is shown in Table I, σ_f and ϵ_f increase significantly after cold drawing. As an example, the stress–elongation curves for $Cu_{65}Zr_{35}$ amorphous wire (original diameter $\simeq$ 135 μm) before and after drawing are shown in Fig. 7. σ_f and ϵ_f as a function of the reduction in cross-sectional area are

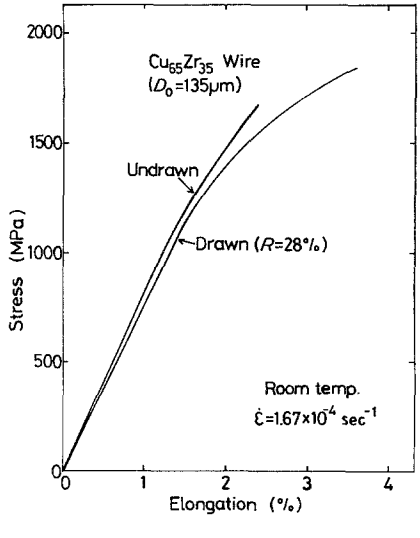

Figure 7 Stress–elongation curves of undrawn and drawn $Cu_{65}Zr_{35}$ amorphous wires.

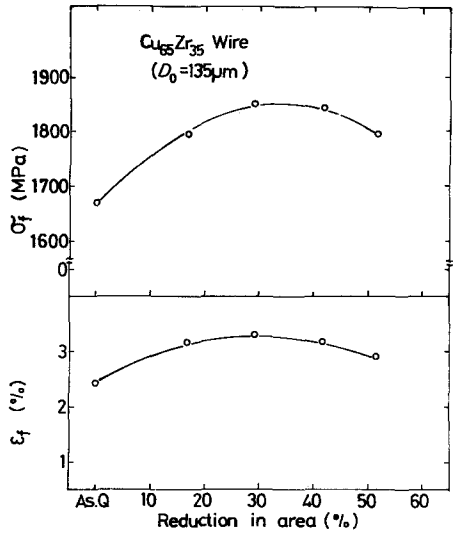

Figure 8 Changes in the tensile strength (σ_f) and elongation to fracture (ϵ_f) of $Cu_{65}Zr_{35}$ amorphous wire with reduction in area.

plotted in Fig. 8. σ_f is about 1670 MPa for the undrawn state and increases gradually with increasing reduction in area. The highest value of 1850 MPa is obtained for 25% to 35% reduction and tends to decrease again with further reduction. Similarly, ϵ_f increases from about 2.4% to 3.3% by light drawing until about 30% reduction. This result indicates that there is an optimum reduction in wire cross-section which results in high strength and large elongation. The strength and elongation of the cold-drawn Cu–Zr amorphous wires shown in Table I are the values after optimized drawing. Additionally, one can see in Fig. 7 that the cold-drawing to 28% reduction in area results in a decrease in Young's modulus (E) by about 7.3%. Such changes in the mechanical properties (σ_f, ϵ_f and E) before and after drawing are similar to those for a number of metal–metalloid type amorphous wires such as Fe–Si–B [1], Fe–P–C [2], Co–Si–B [3], Pd–Ni–Si [4], Pd–Cu–Si [5], Pd–Ni–P [4] and Pt–Ni–P [4]. The significant increases in σ_f and ϵ_f by cold drawing are not caused by a structural change in the amorphous phase but seem to result from the following two factors:

1. the inhibition of the progress of slip displacement by the interaction between the numerous deformation bands introduced by drawing; and

2. the increase in the uniformity of shape due to cold drawing.

In addition, the decreases in σ_f and ϵ_f due to heavy drawing are considered to be caused mainly by the occurrence of cracks or voids at the intersecting points of deformation bands.

3.5. Fracture morphology

The tensile fracture appearance of the undrawn $Cu_{65}Zr_{35}$ amorphous wire is shown in Fig. 9. Tensile fracture occurs on a shear plane at 45° to 50° to the transverse direction of the wire and the morphology of the fracture surface is composed of two distinguishable zones. One is a relatively featureless zone (A) produced by shear slip, and the other (B) is a vein pattern produced by the rupture of the cross-section remaining after the initial shear displacement. This indicates that the fracture of the nonferrous amorphous wire exhibiting high strength proceeds by highly localized shear deformation which contrasts with the brittle fracture without distinct plastic elongation commonly observed in optimumly age-hardened high-strength Cu–Be alloys. These features of the fracture appearance for the Cu–Zr amorphous wire are independent of whether or not a wire has been drawn, being similar to those for Cu–Zr amorphous ribbons [21] and many metal–metalloid type amorphous wires.

3.6. Structural relaxation behaviour

With the aim of assessing the difference in the quenched-in structure due to different quenching conditions between the wires produced by the in-

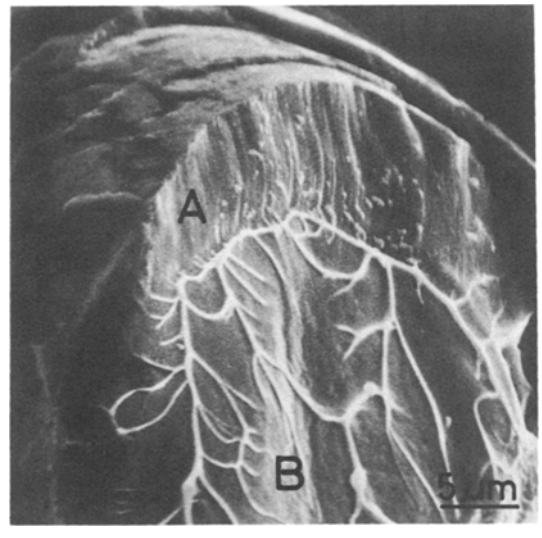

Figure 9 Scanning electron micrograph showing the tensile fracture appearance of undrawn $Cu_{65}Zr_{35}$ amorphous wire.

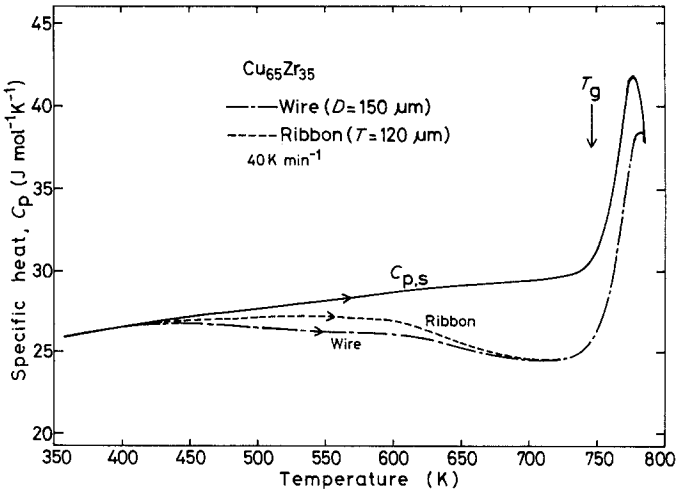

Figure 10 Change in the specific heat (C_p) of an amorphous $Cu_{65}Zr_{35}$ alloy upon heating at a rate of 40 K min^{-1}. —·—, wire of ≃ 150 μm diameter; — — —, ribbon ≃ 120 μm thick.

rotating-water spinning method and the ribbons produced by the conventional single roller melt spinning method, the temperature dependence of the specific heat (C_p) of $Cu_{65}Zr_{35}$ amorphous alloys in the shapes of wire and ribbon was examined with a DSC. As an example, Fig. 10 shows the thermograms of an amorphous $Cu_{65}Zr_{35}$ wire together with the data of an amorphous $Cu_{65}Zr_{35}$ ribbon. The diameter of the wire is about 150 μm and the thickness of the ribbon is about 120 μm. As shown in Fig. 10, C_p of the as-quenched samples began to decrease at about 400 K, indicating that appreciable relaxation occurs even at such a low temperature, i.e. ≃ 150 K below T_g = 747 K. As the temperature rises further, C_p decreases only slightly in the range below 730 K, then rapidly in the region of glass transition and reaches an equilibrium liquid value of about 38.5 J mol^{-1} K^{-1} above 784 K. In the temperature range 420 to 700 K, the apparent specific heat of the as-quenched samples is considerably lower for the wire than for the ribbon.

Fig. 11 shows the temperature dependence of the difference in C_p between the as-quenched and the annealed states [$\Delta C_p(T)$] for the amorphous $Cu_{65}Zr_{35}$ alloy samples of various shapes; wires 80 or 150 μm in diameter and ribbon 120 μm thick. The value of ΔC_p begins to increase at 355 K for the 80 μm wire, at 365 K for the 150 μm wire and at 367 K for the 120 μm ribbon. It increases significantly with rising temperature and reaches a maximum value of 5.0 J mol^{-1} K^{-1} at about 710 to 740 K which is almost the same in all three samples. This figure may be summarized as follows:

1. the temperature at which the structural relaxation begins ($\Delta C_p \gtrsim 0$) is lower for the wire

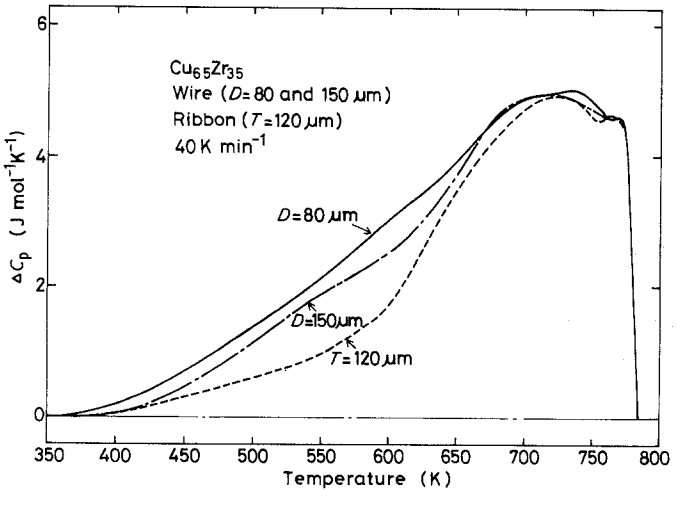

Figure 11 Difference in the specific heat between the as-quenched and annealed state (ΔC_p) for an amorphous $Cu_{65}Zr_{35}$ alloy. ——, wire of ≃ 80 μm diameter; —·—, wire of ≃ 150 μm diameter; — — —, ribbon ≃ 120 μm thick.

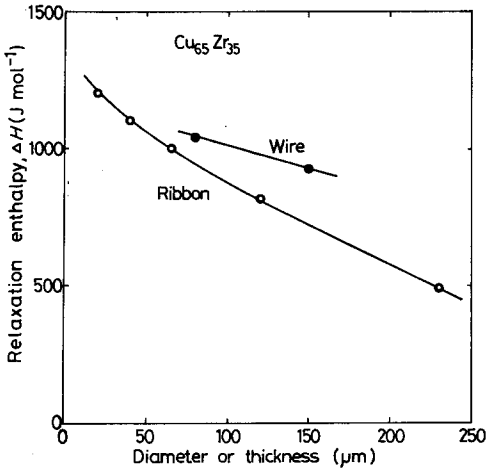

Figure 12 Change in the relaxation enthalpy (ΔH) for an amorphous $Cu_{65}Zr_{35}$ alloy with varying wire diameter and ribbon thickness.

of 80 μm diameter ($\simeq$ 355 K) than for the other samples ($\simeq$ 367 K);

2. ΔC_p in the low temperature region, before merging with each other at about 650 K, is greatest for the wire of 80 μm diameter, followed by the wire having 150 μm diameter and then the ribbon;

3. the integrated heats of relaxation, ΔH, are 1040, 930 and 820 J mol^{-1}, respectively, for wires of 80 and 150 μm diameter and the ribbon.

Fig. 12 shows the relaxation enthalpy of an amorphous $Cu_{65}Zr_{35}$ alloy in the shapes of wire and ribbon as a function of wire diameter or ribbon thickness. When the values of ΔH between the wire and the ribbon are compared at the same values of diameter and thickness, they are seen to be larger for the wires than for the ribbons. Similar differences in $C_p(T)$, $\Delta C_p(T)$ and ΔH have been recognized for Fe–Si–B [22], Fe–P–C [23], Co–Si–B [22], Pd–Ni–P [22] and Pd–Cu–Si [24] amorphous alloys in the shapes of wire and ribbon, and they are interpreted as originating from the inherent differences in the solidification process and the manner of cooling after solidification in the production methods of the wire or ribbon sample, even though the average quench rate which is achieved by each method is considered to be nearly equal in the temperature region near T_g because from the data the values of ΔC_p near T_g are the same for both the wire and ribbon samples. That is, in the case of the in-rotating-water spinning method, cooling of the melt is achieved continuously from the circumferential side by rapidly circulating water. On the other hand, in the single-roller spinning method, solidification of the melt is achieved only through contact with the roller with contacting times and lengths as short as about 0.01 sec and 100 mm [25]. The solidified ribbon detaches itself from the roller above T_g and is air-cooled to room temperature. Consequently, the quench rate from T_g to room temperature is much slower for the ribbon than for the wire. Partial relaxation occurs in the ribbon during air cooling. It manifests itself in the smaller ΔC_p values for the ribbon sample in the low temperature region. Despite the fact that the diameter of the wire is larger than the thickness of the ribbon, the resultant wire possesses higher degrees of structural disorder. This is considered to be the main reason why the present Cu–Zr amorphous wires produced by the in-rotating-water spinning method exhibit a good bending ductility in spite of a diameter as large as about 150 μm.

4. Conclusion

Amorphous wires exhibiting relatively high strength and good bending ductility were produced for the $Cu_{65}Zr_{35}$ and $Cu_{60}Zr_{40}$ alloys having a high amorphous phase-forming ability in the Cu–Zr binary alloy system. The production was carried out using a modified melt-spinning apparatus in which the melt was ejected through the orifice of a quartz nozzle into the rotating water. The amorphous wire diameters obtained are in the range 70 to 150 μm. The wires have a circular cross-section and a rather smooth peripheral surface. Tensile strength (σ_f) and Vickers hardness (H_v) for the undrawn wires tend to increase from 1670 to 1810 MPa and from 425 to 440 DPN, respectively, with decreasing zirconium content. Also, the fracture elongation (ϵ_f) including elastic elongation decreases from 2.7% to 2.4% with decreasing zirconium content. The addition of 5 at % niobium to the $Cu_{65}Zr_{35}$ and $Cu_{60}Zr_{40}$ alloys does not cause a significant detriment to the high amorphous phase-forming ability and the high stability of the ejected jet stream which are essential for the formation of an amorphous wire, and results in increases of σ_f and H_v of about 14% and 4%, respectively, and a decrease in ϵ_f of about 10%. By cold drawing to an appropriate reduction ($\simeq$ 25 to 30%), σ_f and ϵ_f of the $Cu_{65}Zr_{35}$ and $Cu_{60}Zr_{40}$ amorphous wires increase by about 10% and 40%, respectively. Such increases are considered to result from interaction between the

deformation bands introduced by cold drawing, in addition to the increase in the uniformity of shape by drawing. The undrawn amorphous wires are so ductile that no cracks were observed even after a closely contacted bending test. In addition, the good ductility remains unchanged even after heavy cold drawing. The relaxation enthalpy was considerably larger for the wires ($\simeq$ 80 to 150 μm diameter) than for the ribbons ($\simeq$ 60 to 150 μm thick) mainly due to the larger heat evolution at lower temperatures for the former. Furthermore, the temperature of the onset of structural relaxation is lower for the amorphous wires. These results indicate that the structure of the amorphous wires is of a higher degree of frozen-in disorder. The difference was interpreted as originating from the inherent differences in the solidification process of the ejected melt as well as the manner of cooling after solidification.

References

1. M. HAGIWARA, A. INOUE and T. MASUMOTO, *Met. Trans.* **13** (1982) 373.
2. A. INOUE, M. HAGIWARA and T. MASUMOTO, *J. Mater. Sci.* **17** (1982) 580.
3. M. HAGIWARA, A. INOUE and T. MASUMOTO, *Mater. Sci. Eng.* **54** (1982) 197.
4. A. INOUE, Y. MASUMOTO, N. YANO and T. MASUMOTO, *J. Mater. Sci.* in press.
5. T. MASUMOTO, I. OHNAKA, A. INOUE and M. HAGIWARA, *Scripta Metall.* **15** (1981) 293.
6. A. INOUE, H. S. CHEN, J. T. KRAUSE, T. MASUMOTO and M. HAGIWARA, *J. Mater. Sci.* **18** (1983) 2743.
7. I. OHNAKA, T. FUKUSAKO and T. DAIDO, *J. Japan Inst. Metals* **45** (1981) 751.
8. T. MASUMOTO, A. INOUE, M. HAGIWARA, I. OHNAKA and T. FUKUSAKO, Proceedings of the 4th International Conference on Rapidly Quenched Metals, Sendai, August 1981, Vol. 1, edited by T. Masumoto and K. Suzuki (The Japan Institute of Metals, Sendai, 1982) p. 47.
9. H. S. CHEN, R. C. SHERWOOD, S. JIN, G. C. CHI, A. INOUE, T. MASUMOTO and M. HAGIWARA, *J. Appl. Phys.* **55** (1984) 1796.
10. A. INOUE and T. MASUMOTO, *Engng Mater.* **30** (5) (1982) 47, in Japanese.
11. M. HAGIWARA, A. INOUE and T. MASUMOTO, *Met. Trans.* **12A** (1981) 1027.
12. *Idem*, *Sci. Rep. Res. Inst. Tohoku Univ.* **A-29** (1981) 351.
13. M. H. COHEN and D. TURNBULL, *Nature* **189** (1961) 131.
14. D. TURNBULL, *Contemp. Phys.* **10** (1969) 473.
15. H. A. DAVIES, "Rapidly Quenched Metals III", edited by B. Cantor, Vol. 1 (The Metals Society, London, 1978) p. 1.
16. M. NAKA, Y. NISHI and T. MASUMOTO, *ibid.* p. 231.
17. Y. NISHI, K. SUZUKI and T. MASUMOTO, Proceedings of the 4th International Conference on Rapidly Quenched Metals, Sendai, August 1981, Vol. 1; edited by T. Masumoto and K. Suzuki (The Japan Institute of Metals, Sendai, 1982) p. 217.
18. H. S. CHEN, *Acta Metall.* **22** (1974) 897.
19. D. TURNBULL, *J. Phys. Colloque-4* **35** (1974) 1.
20. "Metals Databook" (The Japan Institute of Metals, Maruzen, Tokyo, 1974) p. 156.
21. S. TOMIZAWA and T. MASUMOTO, *Sci. Rep. Res. Inst. Tohoku Univ.* **A-26** (1977) 263.
22. A. INOUE, T. MASUMOTO, M. HAGIWARA and H. S. CHEN, *Scripta Metall.* **17** (1983) 1205.
23. *Idem*, unpublished research (1982).
24. A. INOUE, H. S. CHEN and T. MASUMOTO, *J. Non.-Cryst. Solids* **61/62** (1984) 949.
25. Y. ISHIHARA, private communication, Hitachi Research Laboratory, Hitachi Ltd, Hitachi 317, Japan, August 1981.

Received 20 January
and accepted 30 January 1984